ACS OMEGA

http://pubs.acs.org/journal/acsodf

Article

Non-Mulberry Silk Fiber-Based Composite Scaffolds Containing Millichannels for Auricular Cartilage Regeneration

Xiaoyan Yao, Yuzhou Yang, and Zhimin Zhou*

Cite This: *ACS Omega* 2022, 7, 15064−15073

Read Online

ACCESS | Metrics & More | Article Recommendations

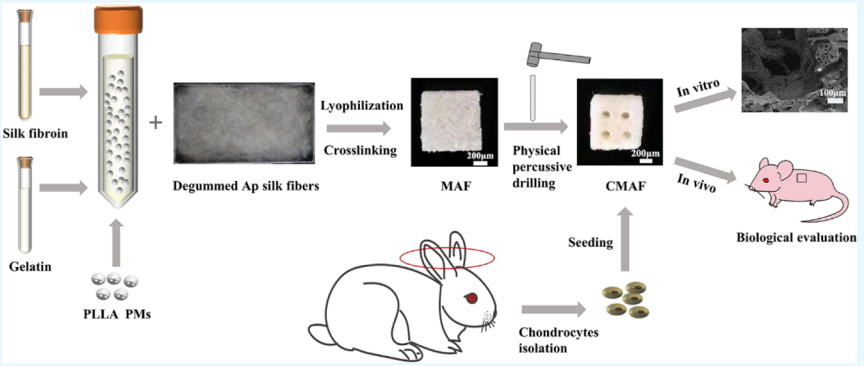

ABSTRACT: Tissue engineering has made significant progress as a cartilage repair alternative. It is crucial to promote cell proliferation and migration within three-dimensional (3D) bulk scaffolds for tissue regeneration through either chemical gradients or physical channels. In this study, by developing optimized silk fiber-based composite scaffolds, millimeter-scaled channels were created in the corresponding scaffolds via facile physical percussive drilling and subsequently utilized for auricular cartilage regeneration. We found that by the introduction of poly-L-lactic acid porous microspheres (PLLA PMs), the channels incorporated into the *Antheraea pernyi* (Ap) silk fiber-based scaffolds were reinforced, and the mechanical features were well maintained. Moreover, Ap silk fiber-based scaffolds reinforced by PLLA PMs containing channels (CMAF) exhibited excellent chondrocyte proliferation, migration, and synthesis of cartilage-specific extracellular matrix (ECM) *in vitro*. The biological evaluation *in vivo* revealed that CMAF had a higher chondrogenic capability for an even deposition of the specific ECM component. This study suggested that multihierarchical CMAF may have potential application for auricular cartilage regeneration.

1. INTRODUCTION

Auricular reconstruction for microtia generally relies on either the gold standard of the autologous rib cartilage technique or auricular prostheses implantation in the clinic.[1−3] Innate limitations, including donor-site morbidity and extrusion or rejection for long-term implantation, have stimulated us to develop alternative strategies for cartilage regeneration. Cartilage tissue engineering provides a promising pathway to overcome the aforementioned limitations.[4−7] In the case of cartilage regeneration, various biomaterials, including collagen, gelatin, silk, hyaluronic acid, poly-L-lactic acid (PLLA), polyglycolic acid, poly(lactic acid-*co*-glycolic acid), and polycaprolactone, have been employed to construct tissue-engineering scaffolds, which provide similar microenvironments to mimic the intrinsic extracellular matrix (ECM).[6,8,9] In addition, mechanical features and porous or channeled structures have significant influence on cell adhesion, proliferation, migration, and differentiation.[9−13] Generally, physical composite techniques or 3D printing is used to prepare polymeric scaffolds with desired physicochemical features to achieve cell seeding and subsequent tissue regeneration.[6,9,10] Previously, in our group, we prepared silk fiber-based composite scaffolds by integrating natural macromolecules [gelatin, silk fibroin, and *Antheraea pernyi* (Ap) silk fiber] with PLLA porous microspheres (PMs) stimulated by a "steel bar reinforced concrete" structure. Such scaffolds offer distinct mechanical properties close to those of native auricular cartilage and have excellent multihierarchical porous structures.[9,10,14] In addition, silk fibroin with basic amino acids and gelatin rich in Arginyl−Glycyl-Aspartic acid (RGD) sequences favored chondrocyte adhesion.[15,16] More importantly, we found that scaffolds consisting of Ap silk fibers demonstrated

Received: February 10, 2022
Accepted: April 7, 2022
Published: April 20, 2022

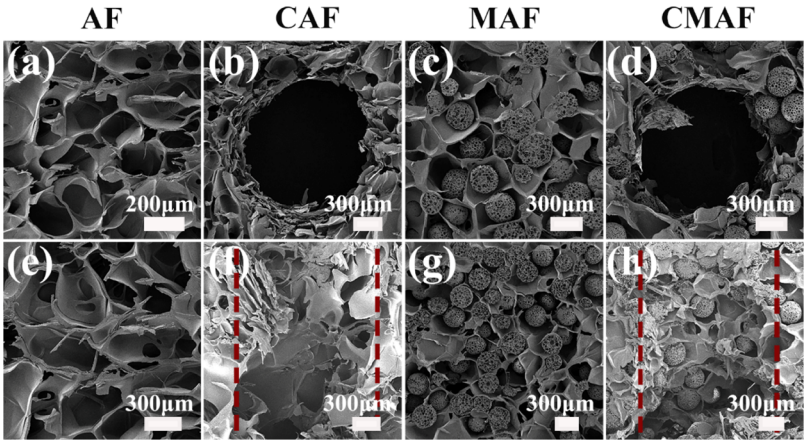

Figure 1. SEM images of the cross sections and vertical sections of (a,e) AF, (b,f) CAF, (c,g) MAF, and (d,h) CMAF.

superior chondrocyte adhesion, proliferation, and glycosaminoglycan (GAG) secretion than their *Bombyx mori* (Bm) silk-based counterparts due to both mechanical advantages and RGD sequences in silk from non-mulberry wild species.[9,15] Nevertheless, the chondrocytes seeded on the silk fiber-based composite scaffolds could not infiltrate into the scaffolds and only formed a layer of cartilage film on the surface. Therefore, it is necessary to guide seed cells to migrate from the surface to the inner section and distribute uniformly in silk fiber-based composite scaffolds to achieve optimized auricular cartilage regeneration.

In fact, the efficiency of cell migration and proliferation in the scaffolds plays an important role in subsequent tissue regeneration. Generally, there are two categories to promote cell ingrowth in scaffolds. From the chemistry point of view, these cellular behaviors were generally manipulated through signal molecule incorporation into scaffolds.[17,18] On the other hand, physical characteristics, including the pore size, topology, and mechanics of scaffolds, as well as culture types affect cell infiltration, migration, and tissue ingrowth.[10,12,19,20] In particular, various physical channels have been created in scaffolds to realize optimal tissue regeneration in the field of cartilage and vascularized artificial tissues due to sufficient nutrient supply.[21−23] For cartilage regeneration, the natural decellularized cartilage-derived matrix enables cell migration throughout the scaffold followed by matrix deposition along the channels.[21,22] As a typical ECM-derived biomaterial, collagen is usually utilized to blend with other organic or inorganic materials to provide cellular attachment sites and the desired mechanics for scaffolds. Oriented channels within the collagen-based scaffolds improved cell migration and infiltration for the optimized regeneration of osteochondral defects.[13,24] Moreover, the repair efficacy of osteochondral defects can be further enhanced by incorporating stromal cell-derived factor-1 or mesenchymal stem cell exosomes in radially oriented scaffolds.[25,26] Similarly, inorganic scaffolds, including hydroxyapatite or β-tricalcium phosphate, could also improve bone tissue regeneration due to favorable cell infiltration and migration from various channels.[17,27,28] It is obvious that physical channels are beneficial for cell seeding and migration followed by tissue ingrowth and regeneration due to nutrient diffusion and spatial access. Therefore, it is important to investigate the effect of physical channels in Ap silk fiber-based scaffolds (AF) and Ap silk fiber-based scaffolds reinforced by PLLA PMs (MAF) on cartilage regeneration.[10,17,19]

In this study, we prepared AF and MAF for auricular cartilage tissue regeneration according to our previously proposed scenario of "steel bar reinforced concrete."[9,10] Then, facile physical percussive drilling was applied to achieve composite scaffolds with vertically ordered channels and to realize a multihierarchical structure ranging from microns of pores of microspheres and bulk scaffolds to milliscale channels.[10,29] Subsequently, the physical features and chondrocyte proliferation and migration were investigated. Finally, chondrogenesis was evaluated primarily *in vivo*.

2. RESULTS AND DISCUSSION

2.1. Fabrication of Silk Fiber-Based Composite Scaffolds. Figure 1 shows the Scanning electron microscopy (SEM) images of the microstructure of silk fiber-based composite scaffolds in cross and vertical sections. We discovered interconnected heterogeneously porous structures in the scaffolds as blank groups without PLLA PM inclusion, and the diameter of the irregular pores produced by gelatin lyophilization was approximately 300−600 μm. The PLLA PMs, as one component for reinforcement of the scaffolds, had a spherical structure with interconnected pores. PLLA PMs ranged in size from 270 to 300 μm in diameter, with pore diameters ranging from 19 to 31 μm. The PLLA PMs were distributed adequately throughout the composite scaffolds (Figure 1c,d,g,h). In fact, a multihierarchical structure of the scaffolds made up of microporous microspheres (19−31 μm) and macroporous bulk scaffolds (300−600 μm) was proposed for continuous cell ingrowth. However, the results of cartilage regeneration *in vivo* were unsatisfactory in previous studies.[10,14] Inspired by the physical channels in various scaffolds for the supply and transport of nutrients and oxygen,[6,13] channels in the range of 1200−1540 μm were manufactured by a custom punch in the composite scaffolds (Figure 1b,d,f,h). Microporous microspheres, macroporous bulk scaffolds, and millimeter-channeled scaffolds were used to realize an optimal and controllable multihierarchical architecture (Figure 1d,h). According to the findings, the scaffold pore size plays a critical role in tissue repair and regeneration as the pore size range and pore geometry can promote particular interactions and affect cell behavior.[19,30] Furthermore, another study found that a large pore size promotes nutrition delivery, whereas a small pore size optimizes cellular interactions.[31] The stiffness of the scaffolds, together with the multihierarchical structure, may

https://doi.org/10.1021/acsomega.2c00846
ACS Omega 2022, 7, 15064−15073

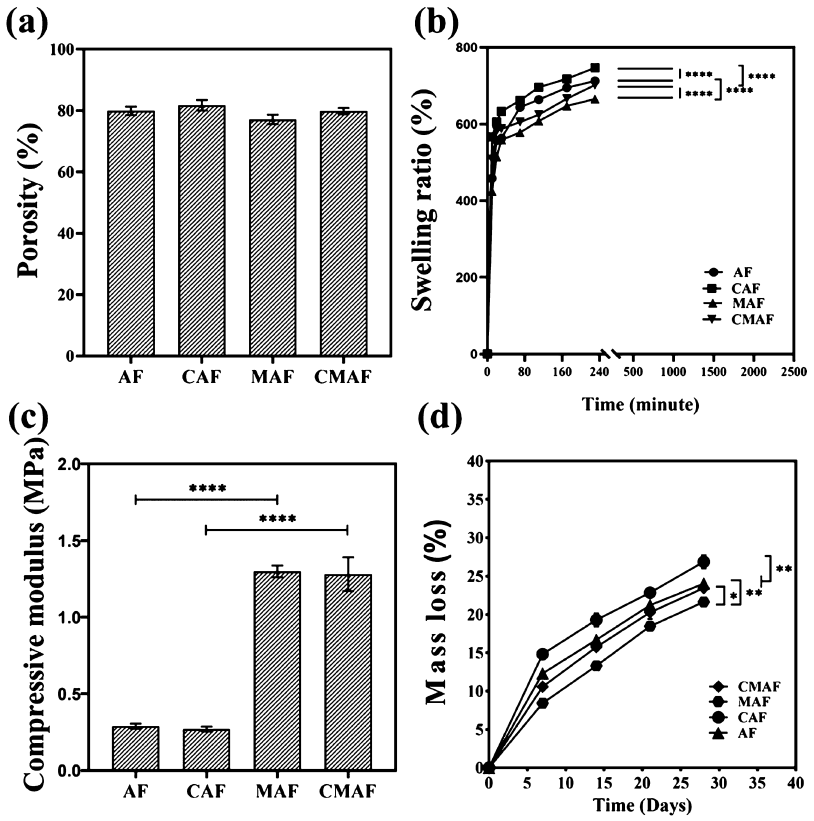

Figure 2. Porosity (a), swelling ratio (b), compressive modulus (c), and mass loss (d) of AF, CAF, MAF, and CMAF.

enhance cell−cell interactions and maintain the chondrocyte phenotype.[32]

2.2. Physical Properties of Silk Fiber-Based Composite Scaffolds. Figure 2a shows that the porosities of AF, Ap silk fiber-based scaffolds containing channels (CAF), MAF, and Ap silk fiber-based scaffolds reinforced by PLLA PMs containing channels (CMAF) were 79.9 ± 1.4, 81.7 ± 1.7, 77.1 ± 1.5, and 79.9 ± 1.0%, respectively. Despite the fact that CAF and CMAF were manufactured as millichannels with a custom-made punch for further study, the porosity showed no significant change. The porosities of AF, CAF, MAF, and CMAF were within the desired range for cell growth and adhesion, indicating that they had appropriate structures for nutrition and waste exchange as well as oxygen diffusion to ensure cell survival.[30]

Swelling behavior is a significant distinguishing feature of scaffolds, serving as a standard for the absorption and storage of large quantities of water.[33] As shown in Figure 2b, the swelling ratios of AF, CAF, MAF, and CMAF were assessed by immersing them in PBS and weighing them at certain time intervals. Despite the fact that all samples revealed swelling, the scaffolds with customized millichannels exhibited superior swelling ability compared to their counterparts. Within 4 h, the scaffolds had absorbed PBS and attained equilibrium. Finally, the swelling ratios of AF, CAF, MAF, and CMAF were estimated to be approximately 712.3, 746.7, 665.3, and 701.9%, respectively, which illustrated that all samples had a good capacity for absorption and storage of liquids. In other words, all composite scaffolds were beneficial for maintaining a moist environment. When composite scaffolds were implanted *in vivo*, the moist environment could promote rapid wound recovery.[34] Certainly, the outstanding swelling behavior of composite scaffolds was mainly attributed to gelatin in the composite scaffolds.[35] According to the literature, gelatin not only has a good ability to absorb and retain liquids but also stimulates the growth of granulation tissue to accelerate wound healing after implantation *in vivo*.[36]

Scaffolds represent physical support for cell proliferation and migration as well as space available for tissue regeneration.[37] Long-term physiologic loads should be maintained by silk fiber-based composite scaffolds.[38] As a result, porous scaffolds should present appropriate architectural and mechanical properties.[29] According to Figure 2c, the compressive modulus of MAF (1.30 ± 0.04 MPa) and CMAF (1.28 ± 0.11 MPa) was significantly higher than that of AF (0.29 ± 0.02 MPa) and CAF (0.27 ± 0.02 MPa). These findings indicated that the mechanical properties of the scaffolds with and without PLLA PMs differed significantly, which was in agreement with our previous studies.[9,10,14] The mechanical properties of scaffolds fabricated by natural biomaterials are inadequate.[39] By the introduction of PLLA PMs, the compressive modulus of the porous scaffolds was enhanced dramatically. MAF and CMAF had mechanical properties similar to those of native auricular cartilage.[40] However, there was no significant change in mechanical properties between scaffolds with and without customized millichannels. In summary, the results revealed that manufacturing customized millichannels in scaffolds (CMAF) did not change the mechanical properties, which allowed shape maintenance during tissue repair and regeneration and enabled stress transfer and load bearing.[37] As reported, reconstruction of auricular cartilage failed frequently owing to a lack of sufficient mechanical properties.[41] Imitating the mechanical properties of native auricular cartilage is the guarantee for composite scaffolds as an alternative to auricular cartilage

https://doi.org/10.1021/acsomega.2c00846
ACS Omega 2022, 7, 15064−15073

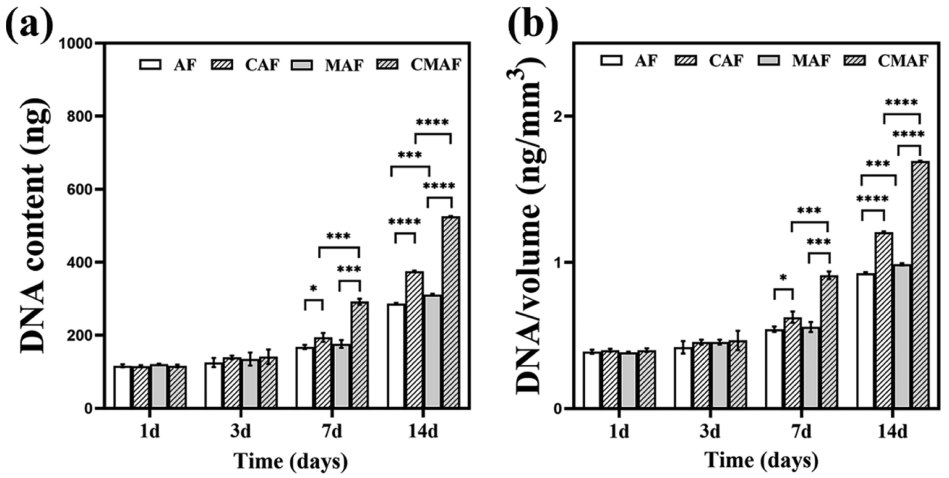

Figure 3. DNA content (a) and scaffold volume-normalized DNA content (b) in AF, CAF, MAF, and CMAF over 28 days.

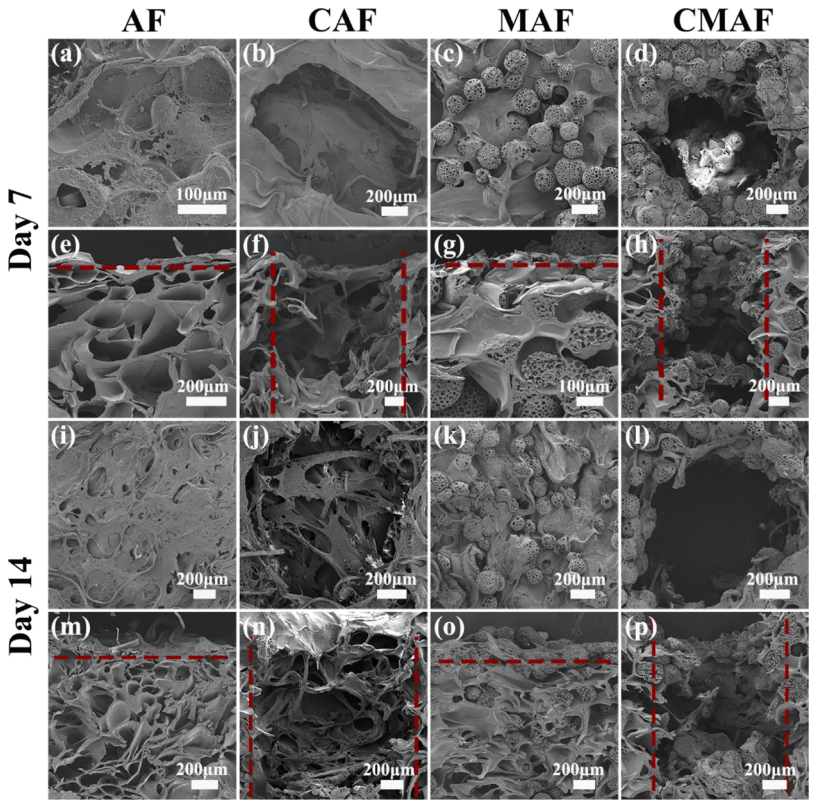

Figure 4. SEM images of the cross sections and vertical sections of chondrocyte morphology: (a,e,i,m) AF, (b,f,j,n) CAF, (c,g,k,o) MAF, and (d,h,l,p) CMAF after culture for 7 and 14 days.

regeneration. Moreover, although the composite scaffolds were designed for auricular cartilage regeneration, they had a promising application in nasal cartilage repair because the amount of PLLA PMs in scaffolds could be adjusted to achieve the mechanical properties required by other damaged cartilage.[10,42]

Since chondrocyte infiltration into composite scaffolds takes several weeks, it is essential for the composite scaffolds to maintain stable function and geometry.[20] In general, the degradation of all samples showed a similar pattern. Within 28 days, the mass losses of AF, CAF, MAF, and CMAF were approximately 24.0, 26.9, 21.6, and 23.4%, respectively (Figure 2d). The ultimate mass loss was within 30%. As the main component of composite scaffolds, gelatin has fast degradability.[35] However, the incorporation of PLLA PMs slowed the mass loss of the scaffolds in the *in vitro* degradation test. In addition, as the component of implantable scaffolds *in vivo*, the slow degradation of PLLA PMs was beneficial to form a slightly acidic microenvironment, which could prevent wound infection directly in favor of the proliferation and effect of immune cells.[34] Moreover, the scaffolds with customized millichannels showed slightly higher degradation. The appropriate degradation guarantees the required support during tissue formation.[37] The scaffolds need a suitable degradability along with adequate mechanical properties to

https://doi.org/10.1021/acsomega.2c00846
ACS Omega 2022, 7, 15064−15073

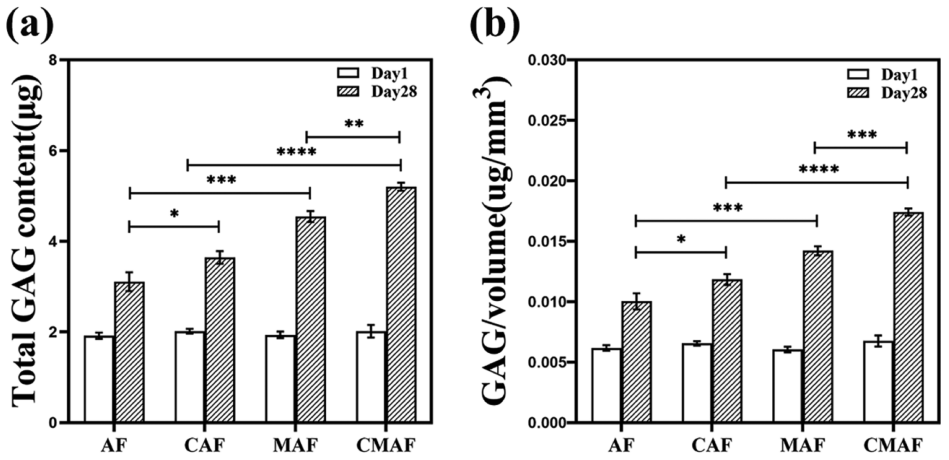

Figure 5. Total GAG content (a) and scaffold volume-normalized GAG content (b) in AF, CAF, MAF, and CMAF on days 1 and 28.

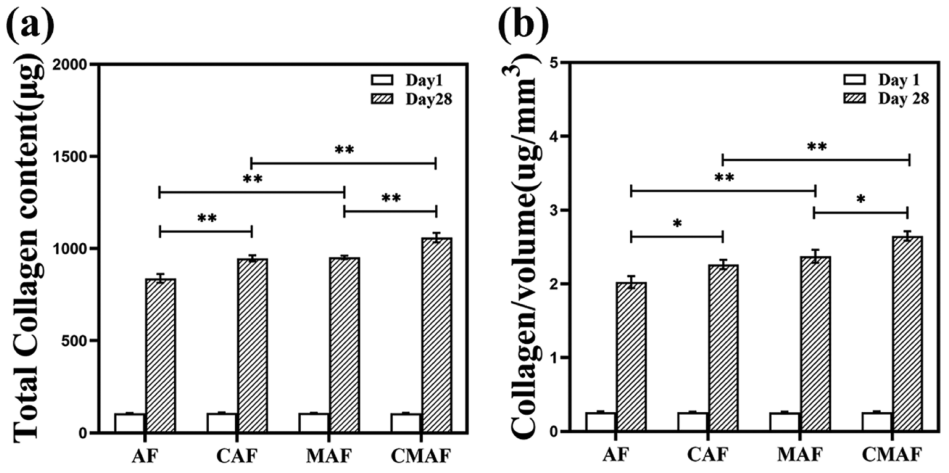

Figure 6. Total collagen content (a) and scaffold volume-normalized collagen content (b) in AF, CAF, MAF, and CMAF on days 1 and 28.

maintain an appropriate appearance during auricular cartilage reconstruction in plastic surgery fields.[10]

2.3. Cell Proliferation Evaluation. Over a period of 14 days, DNA analyses were conducted to assess chondrocyte proliferation in the composite scaffolds. Figure 3a shows that the DNA content on the first day was equal, indicating that the scaffolds seeded chondrocytes at the same level. Although no evident differences were found, the DNA content on the third day was slightly higher than that on the first day. The DNA content of the scaffolds containing customized millichannels (CAF and CMAF) increased on the 7th and 14th days compared with their counterparts (AF and CAF). The DNA content of AF, CAF, MAF, and CMAF increased from approximately 2.5-fold, 3.3-fold, 2.6-fold, and 4.5-fold, respectively, after 14 days of culture when compared to those on day 1 (Figure 3a). This result indicated more chondrocytes inside scaffolds with customized millichannels compared to their counterparts. Therefore, we assumed that the chondrocytes on the surface of CAF and CMAF migrated and proliferated in the millichannels. The DNA contents were normalized to further eliminate differences caused by the scaffold volume, and the normalization of total DNA content with the scaffold volume showed a similar trend. These findings demonstrated that scaffolds containing customized millichannels promoted chondrocyte attachment and proliferation compared to scaffolds without millichannels.[15]

2.4. Cellular Morphology and Distribution in Silk Fiber-Based Composite Scaffolds. The SEM images in Figure 4 display the chondrocyte distribution in AF, CAF, MAF, and CMAF from the cross and vertical sections. A considerable number of chondrocytes proliferated on scaffolds after culturing for 7 days. The chondrocytes were distributed more densely, occupied the irregular pores (300−600 μm) formed by gelatin, completely covered the surface of the scaffolds, and generated larger aggregates on the scaffolds on the 14th day, indicating the existence of ECM.[16] These results may be attributable to the diverse components and multi-hierarchical architecture in silk fiber-based composite scaffolds, which may impact chondrocyte adhesion, distribution, and nutrient diffusion. Although the hydrophobic surface of PLLA PMs in silk fiber-based composite scaffolds has no benefit for cell adherence, the inclusion of silk fibroin and gelatin dramatically enhanced chondrocyte attachment in scaffolds.[15,16] The RGD sequence in the Ap silk architecture was found to provide excellent cell adherence, viability, and proliferation.[9] When the macropore is more than 100 μm, it is beneficial for chondrocytes to congregate and increase chondrocyte−chondrocyte and chondrocyte matrix interactions.[30] Furthermore, chondrocytes were only attached on the top surface for AF and MAF (Figure 4m,o), indicating that in addition to the porosity of the scaffolds, interconnectivity between the pores was essential for cell migration to achieve

https://doi.org/10.1021/acsomega.2c00846
ACS Omega 2022, 7, 15064−15073

high-quality engineered cartilage.[31] In addition, more chondrocytes were found in the millichannels of CAF and CMAF (Figure 4n,p). The results suggested that the physical millichannels supported the migration of chondrocytes into the interior of CMAF and allowed for the exchange of cellular metabolites and nutrients during chondrocyte proliferation.[17] CMAF was found to be effective at promoting cartilage tissue regeneration.

2.5. GAG Secretion Assay. Chondrocytes generate GAGs, which are essential ECM components in the cartilage.[9,43] GAG secretion indicated the ability of the composite scaffolds to generate new ECM.[15] Figure 5a shows that the total GAG content was equal on the first day. However, on day 28, the total GAG content of AF, CAF, MAF, and CMAF showed a considerable increase compared to that on day 1, especially in CMAF. In comparison to their counterparts (AF and CAF), the total GAG content secreted in MAF and CMAF exhibited an increase. Moreover, the total GAG contents of CAF and CMAF were significantly higher than those of AF and MAF. On the 28th day, the content of total GAG increased approximately 1.6-fold, 1.8-fold, 2.3-fold, and 2.6-fold for AF, CAF, MAF, and CMAF, respectively. When the total GAG content was normalized against scaffold volume, a similar trend was seen. All results indicated that the scaffolds with PLLA PMs and customized millimeter channels are beneficial for GAG secretion. Certainly, it has been reported that the microstructure of 3D scaffolds, including the pore size and pore volume, has certain effects on the secretion of ECM and chondrocyte growth.[44] CMAF exhibited a great advantage in cartilage matrix deposition.

2.6. Collagen Secretion Assay. Collagen is the most abundant component of the ECM in cartilage, which provides chondrocytes with a favorable microenvironment.[15,33] Figure 6a indicates that the total collagen content in all composite scaffolds was approximately 106 μg on day 1. After 28 days, the content of collagen in AF, CAF, MAF, and CMAF increased 7.9-fold, 8.7-fold, 8.8-fold, and 9.9-fold, respectively. Similarly, upon normalization with the scaffold volume, the contents of collagen in AF, CAF, MAF, and CMAF were approximately 7.7-fold, 8.7-fold, 9.2-fold, and 10.1-fold, respectively, on day 28. These results suggested that scaffolds containing customized millichannels efficiently promoted the secretion of collagen by chondrocytes, which improved the mechanical properties during the formation of cartilage.[45] CMAF possesses good assistance in the development of high-quality cartilage tissue with abundant collagen.

2.7. *In Vitro* Immunocompatibility. The composite scaffolds can induce an immune response, and an overabundance of this response can result in failure of auricular cartilage regeneration.[9,46] The main orchestrators of the immune response have been identified as macrophages.[47] Therefore, we investigated the tendency of silk fiber-based composite scaffolds to stimulate the secretion of TNF-α from murine macrophage cells. Figure 7 indicates that after 24 h of incubation, the contents of TNF-α in AF, CAF, MAF, and CMAF were comparable to that in the negative control. The results illuminated that the composite scaffolds did not induce any severe immune response, which was in agreement with our previous study.[9] Certainly, this result provided feasibility for *in vivo* experiments.

2.8. *In Vivo* Evaluation of Chondrogenesis. Figure 8a–h show the hematoxylin and eosin (H&E) staining of the chondrocyte distribution in AF, CAF, MAF, and CMAF scaffolds. The CAF and CMAF composite scaffolds showed that a considerable number of chondrocytes were located throughout the scaffolds and aggregated together, whereas chondrocytes were only distributed on the surface of the AF and MAF. More importantly, chondrocytes entered the interior of the CMAF (Figure 8h). Alclan blue staining of the four scaffolds highlighted the deposition of GAGs (Figure 8i–p). More extensive Alclan blue staining occurred on the edge of the AF and MAF (Figure 8i,k). However, GAG deposition was more uniformly distributed in the CAF and CMAF groups (Figure 8j,l). The results were consistent with Figures 4 and 5. Collagen type II was identified in the ECM by immunohistochemistry (IHC). Figure 8q–x reveal that collagen type II was deposited in all composite scaffolds. Nevertheless, collagen type II staining was darker in CAF and CMAF scaffolds. All results illustrated that the CMAF primarily exhibited an outstanding chondrogenic capability for consistent ECM component deposition. Considering that the raw materials of composite scaffolds are commercially available and the preparation process is simple and convenient, we will continue this work in large animals to evaluate the chondrogenic capacity over the long term for auricular cartilage repair and regeneration in the future.

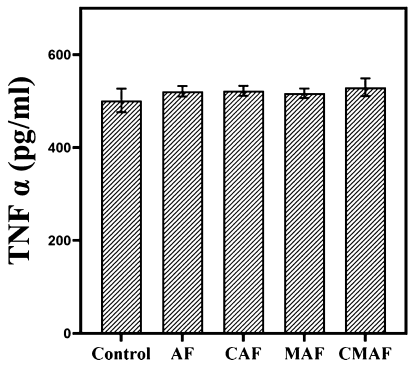

Figure 7. TNF-α release from the mouse macrophage cell line RAW 264.7.

3. CONCLUSIONS

In summary, based on the simple idea of "steel bar reinforced concrete" scaffolds, physical channels were created on Ap silk fiber-based composite scaffolds with no effect on their mechanical features. Compared to the control groups, CMAF, as a stable framework, provided the most appropriate microenvironment to promote chondrocyte migration and synthesis of cartilage-specific ECM in the scaffolds. The proliferation of chondrocytes in the scaffolds was beneficial to the formation of high-quality engineered cartilage. Scaffolds containing physical channels have potential applications in the field of cartilage tissue engineering in the future due to their ability to guide cell migration.

4. MATERIALS AND METHODS

4.1. Materials. The materials used were carboxyl-terminated PLLA (M_w: 50,000, Daigang Biomaterial, Jinan, China), dichloromethane (Tianjin University Kewei Company, China), ammonium bicarbonate (Adamas-β, Shanghai, China), poly(vinyl alcohol) (Sinopec Chongqing Svw Chemical Co., Chongqing, China), gelatin (GeneRun, Tianjin, China), A. pernyi cocoons (Ap silk fibers, Dandong, Liaoning, China), silk fibroin from B. mori cocoons (Beijing Sinolactide Medical

https://doi.org/10.1021/acsomega.2c00846
ACS Omega 2022, 7, 15064−15073

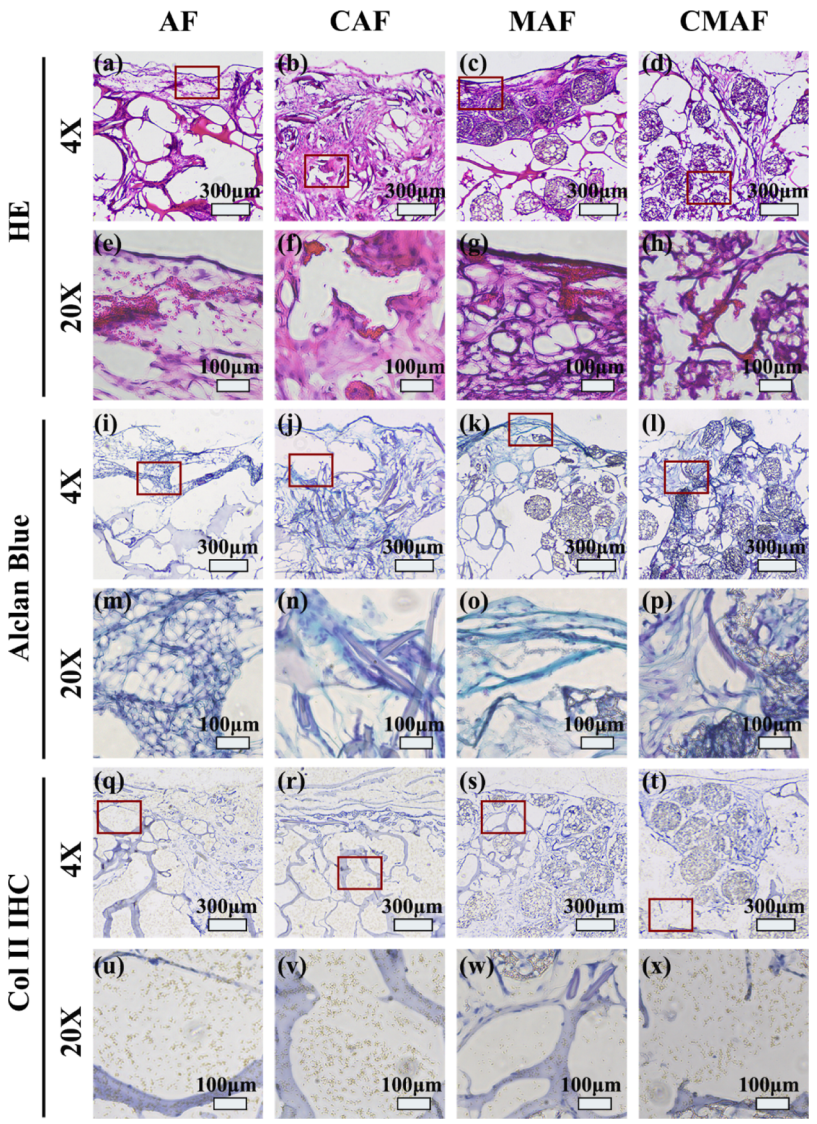

Figure 8. H&E (a–h), Alclan Blue (i–p), and Col II IHC (q–x) staining images of AF, CAF, MAF, and CMAF after cultivation *in vitro* for 4 weeks and *in vivo* for another 4 weeks. The regions corresponding to the magnified stained pictures are shown by red squares.

Technology Co., Beijing, China), high-glucose Dulbecco's modified Eagle's medium (DMEM, HyClone, USA), fetal bovine serum (FBS, Clack, Australia), and a H&E staining kit (Solarbio, Beijing, China). Hoechst 33258 solution (Kumamoto, Japan) and a Mouse TNF alpha Uncoated ELISA Kit were acquired from Invitrogen. Animal Cell Pas Alclan Blue Kit (GENMED, USA) and Collagen II IHC staining kit (GENMED, USA) were also used.

4.2. Fabrication of Silk Fiber-Based Composite Scaffolds Containing Millichannels. Degummed Ap silk fibers and PLLA PMs were obtained first according to our previous study.[9] Then, the dispersed solution (15 mL) was produced by combining aqueous solution silk fibroin (45 mg), gelatin (1.35 g), and PLLA PMs (0 or 200 mg). Subsequently, to make the composites, the dispersion solution and degummed Ap silk mesh (40 mg) were physically blended and vacuum freeze-dried. The composites were cross-linked with EDC solution for 8 h, washed 3 times with distilled water, and freeze-dried. Finally, the composite scaffolds, including AF and MAF, were obtained and sliced into small cuboids (10 mm × 10 mm × 4 mm). To obtain composite scaffolds containing millichannels, a custom-made punch was used to realize CAF and CMAF.

4.3. Characterization of the Scaffolds. *4.3.1. Morphologies and Porosity.* A scanning electron microscope (ZEISS, Germany) was applied to examine the morphologies of AF, CAF, MAF, and CMAF in both vertical and cross-sectional directions. The samples were sputter-coated with gold. Furthermore, the images were analyzed by ImageJ software. The pore sizes of AF, CAF, MAF, and CMAF were measured from the horizontal cross section of the composite scaffolds using different SEM images (n = 3). The porosity was assessed by examining the percentage area of the scaffold surface occupied by the pores compared to the entire visible cross-sectional area of the photograph.[15]

4.3.2. Swelling Behavior of Scaffolds. We weighed the dry scaffolds (W_d) before immersing the samples entirely in PBS at 37 °C. The hydrated scaffolds were recorded (W_w) at predefined time intervals after the liquid on the surface was removed. The following equation was used to estimate the swelling ratio

https://doi.org/10.1021/acsomega.2c00846
ACS Omega 2022, 7, 15064−15073

$$\text{swelling ratio}(\%) = (W_W - W_d)/W_d \times 100\%$$

4.3.3. Mechanical Measurement. To evaluate the mechanical properties of AF, CAF, MAF, and CMAF, a universal material testing machine (INSTRON, USA) was utilized in this study. Prior to the test, the cuboid-shaped scaffolds were incubated in PBS for 30 min at 37 °C. After the liquid of the scaffolds on the surface was wiped gently, the length, width, and height of all samples were noted. The compression speed was set at 1 mm/min, and the experiments were repeated until the sample height was reduced by 50%.

4.3.4. Degradation Test In Vitro. To examine the degradation of all scaffolds, the scaffolds were immersed in PBS and shaken at 37 °C and 100 rpm, and the weight (m_0) was recorded. PBS was refreshed every 3 days. The scaffolds were lyophilized and weighed (m_t) on days 7, 14, 21, and 28 after being cleaned three times with distilled water (m_t). The following equation was used to calculate the mass loss ratio of the scaffolds

$$\text{mass loss ratio}(\%) = (m_0 - m_t)/m_0 \times 100\%$$

4.4. Chondrocyte Isolation, Proliferation, and Seeding on the Scaffolds. All of the procedures in this study were performed with permission from the Animal Ethical and Welfare Committee of the Experimental Animal Center of the Institution of Radiation Medicine, Chinese Academy of Medical Science. Six 5-week-old rabbits were sacrificed to harvest fresh chondrocytes. After a series of treatments of the rabbit ears, the auricular cartilages were sliced into pieces under sterile circumstances and then digested with trypsin (0.25%) for 30 min and type IV collagenase (0.2%) for 2−4 h at 37 °C. Finally, the dispersion was filtered, centrifuged, and resuspended in the culture medium, which consisted of DMEM, FBS (10%), and penicillin−streptomycin solution (1%). The cells were trypsinized and subcultured in new Petri dishes when they reached 80−90% confluency. We utilized P2 rabbit chondrocytes in this study. The sterilized scaffolds were soaked in DMEM for 1 h. The samples for the four groups were seeded with chondrocyte suspension (1×10^7/mL, 100 μL). All samples were given culture medium (1 mL) after 4 h of incubation, and the medium was refreshed every 2 days.

4.5. *In Vitro* Biological Evaluation. *4.5.1. Cell Proliferation.* The total DNA content was quantified using the Animal Tissues/Cells Genomic DNA Extraction kit (Solarbio, Beijing, China) to quantify chondrocyte proliferation on the composite scaffolds. In summary, scaffold-seeded chondrocytes were digested and subjected to a variety of elution procedures. Both DNA samples (20 μL) and Hoechst 33258 solution (0.2% V/V) (180 μL) were added to a 96-well plate, followed by incubation away from light for 5 min, and the fluorescence was detected at 356/492 nm (excitation/emission). To minimize scaffold size differences, the DNA content of the composite scaffolds was determined using the standard curve and normalized against the scaffold volume.

4.5.2. Cell Morphology and Distribution. The cell-laden scaffolds were washed gently with PBS and soaked in 4% paraformaldehyde for 2 h to investigate the morphology and distribution of chondrocytes on the composite scaffolds cultivated for 7 and 14 days. All samples were instantly dried using the critical point drying technique after they were dehydrated with ethanol and isoamyl acetate. Finally, the chondrocytes on the scaffolds were sprayed with gold and examined by SEM.

4.5.3. GAG Secretion Assay. The content of GAGs secreted in the composite scaffolds was assessed using the Cell GAG Total Content DMMB Colorimetry Kit (GENMED, USA) according to the manufacturer's guidelines. The scaffolds were digested for 16 h in total. The GAG sample was treated with the DMMB reagent. After vortex movement for 15 s, incubation at room temperature for 30 min, centrifugation, and removal of the supernatant liquid, propanol solution was added, and the absorbance was detected at 656 nm. To remove scaffold size discrepancies, the contents of GAGs on the composite scaffolds were quantified using the standard curve and normalized against the scaffold volume.

4.5.4. Collagen Secretion Assay. Throughout the Sircol Soluble Collagen Assay (Biocolor, Britain), the total collagen content was measured. In short, pepsin (0.1 mg/mL) was applied to composite scaffolds for 48 h at 4 °C. The samples were centrifuged after the addition of Isolation & Concentration Reagent and placed at 4 °C overnight. Subsequently, the supernatant liquid was combined with Sircol Dye Reagent and shaken for 30 min at room temperature. Ice-cold acid-salt wash reagent was added to the collagen-dye pellet after centrifugation and removal of the supernatant liquid. All samples were centrifuged again. Finally, alkali reagent was added to dissolve all of the bound dye. The absorbance was recorded at 555 nm. The composite scaffold cultured without seed chondrocytes was used as the blank group. To eliminate scaffold size discrepancies, the contents of collagen on the composite scaffolds were measured by the standard curve provided by the kit and normalized against the scaffold volume.

4.5.5. In Vitro Immunocompatibility. The immunocompatibility of AF, CAF, MAF, and CMAF was evaluated with the murine macrophage cell line (RAW 264.7). The spent medium without scaffolds was regarded as the negative control. After the incubation of the scaffolds and RAW 264.7 cells for 24 h, the spent medium was collected and analyzed for TNF-α using a Mouse TNF alpha Uncoated ELISA Kit. In brief, 50 μL/well of detection antibody was added to a 96-well plate that contained the combination of samples and capture antibodies and incubated for 1 h. After three washes, diluted streptavidin-HRP was added and incubated for 30 min. Each washed well was filled with chromogen (TMB) solution and incubated in the dark for 15 min. Finally, with the addition of the stop solution, the content of TNF-α was measured at the absorbance of 450 nm.

4.6. *In Vivo* Chondrogenesis Estimation in Nude Mice. All of the procedures in this experiment were performed with permission from the Animal Ethical and Welfare Committee of the Experimental Animal Center of the Institution of Radiation Medicine, Chinese Academy of Medical Sciences. In the experiment, 12 female BALB/c nude mice that were 5 weeks old, which weighed between 16 and 22 g, were divided into two groups at random to assess the *in vivo* compatibility and chondrogenesis potential. The cell-laden scaffolds (AF, CAF, MAF, and CMAF) were implanted *in vitro* for 4 weeks into the nude mice subcutaneously. Specifically, the AF and CAF were implanted in the left- and right-hand sides of the first group of mice. Similarly, the mice in the second group were implanted with MAF in the left side and CMAF in the right side. For the duration of the experiment, all mice were maintained under IVC conditions. The nude mice were sacrificed at 4 week intervals to extract the scaffolds for further study. The scaffolds were fixed in 4% paraformaldehyde for 48 h and then dehydrated in 30% sucrose aqueous solution for 3 days before

https://doi.org/10.1021/acsomega.2c00846
ACS Omega 2022, 7, 15064−15073

being embedded in the optimal cutting temperature compound. Finally, a microtome (Leica, Germany) was employed to cut vertical slices with a 5 μm thickness. The distribution of chondrocytes was shown using H&E staining, the deposition of sulfated proteoglycans was evaluated using the Animal Cell Pas Alclan Blue Kit, and collagen II was observed using the Collagen II IHC staining kit.

4.7. Statistical Analysis. Data were plotted as the mean ± standard deviation ($n = 3$). SPSS Statistics 26.0 software (IBM, USA) was used to evaluate quantitative data. Statistical significance was defined at $p < 0.05$ ($^{*}P < 0.05$, $^{**}P < 0.01$, $^{***}P < 0.001$).

AUTHOR INFORMATION

Corresponding Author

Zhimin Zhou − *Biomedical Barriers Research Center, Institute of Biomedical Engineering, Chinese Academy of Medical Sciences & Peking Union Medical College, Tianjin 300192, China;* orcid.org/0000-0003-4832-3530; Email: zhouzm@bme.cams.cn, zhouzhiminf@126.com

Authors

Xiaoyan Yao − *Biomedical Barriers Research Center, Institute of Biomedical Engineering, Chinese Academy of Medical Sciences & Peking Union Medical College, Tianjin 300192, China*

Yuzhou Yang − *Biomedical Barriers Research Center, Institute of Biomedical Engineering, Chinese Academy of Medical Sciences & Peking Union Medical College, Tianjin 300192, China*

Complete contact information is available at: https://pubs.acs.org/10.1021/acsomega.2c00846

Notes

The authors declare no competing financial interest.

ACKNOWLEDGMENTS

This work was supported by grants from the CAMS Innovation Fund for Medical Sciences (2021-I2M-1-052), the Tianjin Natural Science Foundation (19JCYBJC29300), the Hygiene and Health Development Scientific Research Fostering Plan of Haidian District Beijing (HP2021-11-80603), and the Peking Union Medical College Subject Construction Program for the "Science for Biomedical Barriers" (201920201501).

REFERENCES

(1) Cubitt, J. J.; Chang, L. Y.; Liang, D.; Vandervord, J.; Marucci, D. D. Auricular reconstruction. *J. Paediatr. Child Health* **2019**, *55*, 512−517.

(2) Jiang, H.; Pan, B.; Lin, L.; Cai, Z.; Zhuang, H. Ten-year experience in microtia reconstruction using tissue expander and autogenous cartilage. *Int. J. Pediatr. Otorhinolaryngol.* **2008**, *72*, 1251−1259.

(3) Humphries, S.; Joshi, A.; Webb, W. R.; Kanegaonkar, R. Auricular reconstruction: where are we now? A critical literature review. *Eur. Arch. Oto-Rhino-Laryngol.* **2022**, *279*, 541−556.

(4) Sterodimas, A.; de Faria, J.; Correa, W. E.; Pitanguy, I. Tissue engineering and auricular reconstruction: a review. *J. Plast. Reconstr. Aesthetic Surg.* **2009**, *62*, 447−452.

(5) Zhou, G.; Jiang, H.; Yin, Z.; Liu, Y.; Zhang, Q.; Zhang, C.; Pan, B.; Zhou, J.; Zhou, X.; Sun, H.; et al. In Vitro Regeneration of Patient-specific Ear-shaped Cartilage and Its First Clinical Application for Auricular Reconstruction. *EBioMedicine* **2018**, *28*, 287−302.

(6) Kang, H.-W.; Lee, S. J.; Ko, I. K.; Kengla, C.; Yoo, J. J.; Atala, A. A 3D bioprinting system to produce human-scale tissue constructs with structural integrity. *Nat. Biotechnol.* **2016**, *34*, 312−319.

(7) Uto, S.; Hikita, A.; Sakamoto, T.; Mori, D.; Yano, F.; Ohba, S.; Saito, T.; Takato, T.; Hoshi, K. Ear Cartilage Reconstruction Combining Induced Pluripotent Stem Cell-Derived Cartilage and Three-Dimensional Shape-Memory Scaffold. *Tissue Eng., Part A* **2021**, *27*, 604−617.

(8) Armiento, A. R.; Stoddart, M. J.; Alini, M.; Eglin, D. Biomaterials for articular cartilage tissue engineering: Learning from biology. *Acta Biomater.* **2018**, *65*, 1−20.

(9) Yang, Y.; Yao, X.; Li, X.; Guo, C.; Li, C.; Liu, L.; Zhou, Z. Non-mulberry silk fiber-based scaffolds reinforced by PLLA porous microspheres for auricular cartilage: An in vitro study. *Int. J. Biol. Macromol.* **2021**, *182*, 1704−1712.

(10) Zeng, Y.; Li, X.; Liu, X.; Yang, Y.; Zhou, Z.; Fan, J.; Jiang, H. PLLA Porous Microsphere-Reinforced Silk-Based Scaffolds for Auricular Cartilage Regeneration. *ACS Omega* **2021**, *6*, 3372−3383.

(11) Stenhamre, H.; Nannmark, U.; Lindahl, A.; Gatenholm, P.; Brittberg, M. Influence of pore size on the redifferentiation potential of human articular chondrocytes in poly(urethane urea) scaffolds. *J. Tissue Eng. Regener. Med.* **2011**, *5*, 578−588.

(12) Nava, M. M.; Draghi, L.; Giordano, C.; Pietrabissa, R. The effect of scaffold pore size in cartilage tissue engineering. *J. Appl. Biomater. Funct. Mater.* **2016**, *14*, e223−e229.

(13) Seong, Y.-J.; Kang, I.-G.; Song, E.-H.; Kim, H.-E.; Jeong, S.-H. Calcium Phosphate-Collagen Scaffold with Aligned Pore Channels for Enhanced Osteochondral Regeneration. *Adv. Healthcare Mater.* **2017**, *6*, 1700966.

(14) Li, T.; Liu, B.; Jiang, Y.; Lou, Y.; Chen, K.; Zhang, D. L-polylactic acid porous microspheres enhance the mechanical properties and in vivo stability of degummed silk/silk fibroin/gelatin scaffold. *Biomed. Mater.* **2020**, *16*, 015025.

(15) Singh, Y. P.; Bandyopadhyay, A.; Mandal, B. B. 3D Bioprinting Using Cross-Linker-Free Silk-Gelatin Bioink for Cartilage Tissue Engineering. *ACS Appl. Mater. Interfaces* **2019**, *11*, 33684−33696.

(16) Ju, H. W.; Sheikh, F. A.; Moon, B. M.; Park, H. J.; Lee, O. J.; Kim, J. H.; Eun, J. J.; Khang, G.; Park, C. H. Fabrication of poly(lactic-co-glycolic acid) scaffolds containing silk fibroin scaffolds for tissue engineering applications. *J. Biomed. Mater. Res., Part A* **2014**, *102*, 2713−2724.

(17) Yang, D.; Zhao, Z.; Bai, F.; Wang, S.; Tomsia, A. P.; Bai, H. Promoting Cell Migration in Tissue Engineering Scaffolds with Graded Channels. *Adv. Healthcare Mater.* **2017**, *6*, No. e1700472.

(18) Zhang, T.; Li, M.; Wang, X.; Zhou, Z.; Yuan, W.; Ma, J. Facile synthesis of polylactide coarse microspheres as artificial antigen-presenting cells. *Chem. Commun.* **2018**, *54*, 11356−11359.

(19) Sgarminato, V.; Tonda-Turo, C.; Ciardelli, G. Reviewing recently developed technologies to direct cell activity through the control of pore size: From the macro- to the nanoscale. *J. Biomed. Mater. Res., Part B* **2020**, *108*, 1176−1185.

(20) Goldberg-Bockhorn, E.; Wenzel, U.; Theodoraki, M. N.; Doscher, J.; Riepl, R.; Wigand, M. C.; Brunner, C.; Hessling, M.; Hoffmann, T. K.; Kern, J.; et al. Enhanced cellular migration and prolonged chondrogenic differentiation in decellularized cartilage scaffolds under dynamic culture conditions. *J. Tissue Eng. Regener. Med.* **2022**, *16*, 36−50.

(21) Nürnberger, S.; Schneider, C.; van Osch, G. V. M.; Keibl, C.; Rieder, B.; Monforte, X.; Teuschl, A. H.; Mühleder, S.; Holnthoner, W.; Schädl, B.; et al. Repopulation of an auricular cartilage scaffold, AuriScaff, perforated with an enzyme combination. *Acta Biomater.* **2019**, *86*, 207−222.

(22) Rowland, C. R.; Colucci, L. A.; Guilak, F. Fabrication of anatomically-shaped cartilage constructs using decellularized cartilage-derived matrix scaffolds. *Biomaterials* **2016**, *91*, 57−72.

(23) Fang, Y.; Ouyang, L.; Zhang, T.; Wang, C.; Lu, B.; Sun, W. Optimizing Bifurcated Channels within an Anisotropic Scaffold for Engineering Vascularized Oriented Tissues. *Adv. Healthcare Mater.* **2020**, *9*, 2000782.

(24) Feng, X.; Xu, P.; Shen, T.; Zhang, Y.; Ye, J.; Gao, C. Influence of pore architectures of silk fibroin/collagen composite scaffolds on the regeneration of osteochondral defects in vivo. *J. Mater. Chem. B* **2020**, *8*, 391−405.
(25) Chen, P.; Tao, J.; Zhu, S.; Cai, Y.; Mao, Q.; Yu, D.; Dai, J.; Ouyang, H. Radially oriented collagen scaffold with SDF-1 promotes osteochondral repair by facilitating cell homing. *Biomaterials* **2015**, *39*, 114−123.
(26) Chen, P.; Zheng, L.; Wang, Y.; Tao, M.; Xie, Z.; Xia, C.; Gu, C.; Chen, J.; Qiu, P.; Mei, S.; et al. Desktop-stereolithography 3D printing of a radially oriented extracellular matrix/mesenchymal stem cell exosome bioink for osteochondral defect regeneration. *Theranostics* **2019**, *9*, 2439−2459.
(27) Bai, H.; Wang, D.; Delattre, B.; Gao, W.; De Coninck, J.; Li, S.; Tomsia, A. P. Biomimetic gradient scaffold from ice-templating for self-seeding of cells with capillary effect. *Acta Biomater.* **2015**, *20*, 113−119.
(28) Wang, X.; Lin, M.; Kang, Y. Engineering Porous beta-Tricalcium Phosphate (beta-TCP) Scaffolds with Multiple Channels to Promote Cell Migration, Proliferation, and Angiogenesis. *ACS Appl. Mater. Interfaces* **2019**, *11*, 9223−9232.
(29) He, F.; Lu, T.; Fang, X.; Feng, S.; Feng, S.; Tian, Y.; Li, Y.; Zuo, F.; Deng, X.; Ye, J. Novel Extrusion-Microdrilling Approach to Fabricate Calcium Phosphate-Based Bioceramic Scaffolds Enabling Fast Bone Regeneration. *ACS Appl. Mater. Interfaces* **2020**, *12*, 32340−32351.
(30) Vila-Parrondo, C.; García-Astrain, C.; Liz-Marzán, L. M. Colloidal systems toward 3D cell culture scaffolds. *Adv. Colloid Interface Sci.* **2020**, *283*, 102237.
(31) Lammi, M.; Piltti, J.; Prittinen, J.; Qu, C. Challenges in Fabrication of Tissue-Engineered Cartilage with Correct Cellular Colonization and Extracellular Matrix Assembly. *Int. J. Mol. Sci.* **2018**, *19*, 2700.
(32) Li, S.; Tallia, F.; Mohammed, A. A.; Stevens, M. M.; Jones, J. R. Scaffold channel size influences stem cell differentiation pathway in 3-D printed silica hybrid scaffolds for cartilage regeneration. *Biomater. Sci.* **2020**, *8*, 4458−4466.
(33) Singh, Y. P.; Bhardwaj, N.; Mandal, B. B. Potential of Agarose/Silk Fibroin Blended Hydrogel for in Vitro Cartilage Tissue Engineering. *ACS Appl. Mater. Interfaces* **2016**, *8*, 21236−21249.
(34) Lei, H.; Zhu, C.; Fan, D. Optimization of human-like collagen composite polysaccharide hydrogel dressing preparation using response surface for burn repair. *Carbohydr. Polym.* **2020**, *239*, 116249.
(35) Chen, Y.; Wu, T.; Huang, S.; Suen, C.-W. W.; Cheng, X.; Li, J.; Hou, H.; She, G.; Zhang, H.; Wang, H.; et al. Sustained Release SDF-1alpha/TGF-beta1-Loaded Silk Fibroin-Porous Gelatin Scaffold Promotes Cartilage Repair. *ACS Appl. Mater. Interfaces* **2019**, *11*, 14608−14618.
(36) Gaspar-Pintiliescu, A.; Stanciuc, A.-M.; Craciunescu, O. Natural composite dressings based on collagen, gelatin and plant bioactive compounds for wound healing: A review. *Int. J. Biol. Macromol.* **2019**, *138*, 854−865.
(37) Carletti, E.; Motta, A.; Migliaresi, C. Scaffolds for tissue engineering and 3D cell culture. *Methods Mol. Biol.* **2011**, *695*, 17−39.
(38) Balakrishnan, B.; Banerjee, R. Biopolymer-based hydrogels for cartilage tissue engineering. *Chem. Rev.* **2011**, *111*, 4453−4474.
(39) Nematollahi, Z.; Tafazzoli-Shadpour, M.; Zamanian, A.; Seyedsalehi, A.; Shadmehr, M.-B.; Ghorbani, F.; Mirahmadi, F. Fabrication of Chitosan Silk-based Tracheal Scaffold Using Freeze-Casting Method. *Iran. Biomed. J.* **2017**, *21*, 228−239.
(40) Bos, E. J.; Pluemeekers, M.; Helder, M.; Kuzmin, N.; van der Laan, K.; Groot, M.-L.; van Osch, G.; van Zuijlen, P. Structural and Mechanical Comparison of Human Ear, Alar, and Septal Cartilage. *Plast. Reconstr. Surg.* **2018**, *6*, No. e1610.
(41) Nimeskern, L.; van Osch, G. J. V. M.; Müller, R.; Stok, K. S. Quantitative evaluation of mechanical properties in tissue-engineered auricular cartilage. *Tissue Eng., Part B* **2014**, *20*, 17−27.
(42) Lavernia, L.; Brown, W. E.; Wong, B. J. F.; Hu, J. C.; Athanasiou, K. A. Toward tissue-engineering of nasal cartilages. *Acta Biomater.* **2019**, *88*, 42−56.
(43) Menezes, R.; Arinzeh, T. L. Comparative Study of Electrospun Scaffolds Containing Native GAGs and a GAG Mimetic for Human Mesenchymal Stem Cell Chondrogenesis. *Ann. Biomed. Eng.* **2020**, *48*, 2040−2052.
(44) Lien, S.-M.; Ko, L.-Y.; Huang, T.-J. Effect of pore size on ECM secretion and cell growth in gelatin scaffold for articular cartilage tissue engineering. *Acta Biomater.* **2009**, *5*, 670−679.
(45) Li, J.; Cao, R.; Wang, Q.; Shi, H.; Wu, Y.; Sun, K.; Liu, X.; Jiang, H. Cadherin-11 promotes the mechanical strength of engineered elastic cartilage by enhancing extracellular matrix synthesis and microstructure. *J. Tissue Eng. Regener. Med.* **2022**, *16*, 188−199.
(46) Yang, D.; Xiao, J.; Wang, B.; Li, L.; Kong, X.; Liao, J. The immune reaction and degradation fate of scaffold in cartilage/bone tissue engineering. *Mater. Sci. Eng., C* **2019**, *104*, 109927.
(47) Taraballi, F.; Sushnitha, M.; Tsao, C.; Bauza, G.; Liverani, C.; Shi, A.; Tasciotti, E. Biomimetic Tissue Engineering: Tuning the Immune and Inflammatory Response to Implantable Biomaterials. *Adv. Healthcare Mater.* **2018**, *7*, No. e1800490.

https://doi.org/10.1021/acsomega.2c00846
ACS Omega 2022, 7, 15064−15073